The University of Maine
DigitalCommons@UMaine

Electronic Theses and Dissertations | Fogler Library

Spring 5-12-2017

Revisiting Ocean Color algorithms for chlorophyll a and particulate organic carbon in the Southern Ocean using biogeochemical floats

Nils Haëntjens
University of Maine, nils.haentjens@maine.edu

Follow this and additional works at: http://digitalcommons.library.umaine.edu/etd

 Part of the Oceanography Commons

Recommended Citation
Haëntjens, Nils, "Revisiting Ocean Color algorithms for chlorophyll a and particulate organic carbon in the Southern Ocean using biogeochemical floats" (2017). *Electronic Theses and Dissertations*. 2654.
http://digitalcommons.library.umaine.edu/etd/2654

This Open-Access Thesis is brought to you for free and open access by DigitalCommons@UMaine. It has been accepted for inclusion in Electronic Theses and Dissertations by an authorized administrator of DigitalCommons@UMaine.

REVISITING OCEAN COLOR ALGORITHMS FOR CHLOROPHYLL *A* AND PARTICULATE ORGANIC CARBON IN THE SOUTHERN OCEAN USING BIOGEOCHEMICAL FLOATS

By

Nils Haëntjens

Master's Degree in Embedded Systems, ISEP, 2015

A THESIS

Submitted in Partial Fulfillment of the

Requirements for the Degree of

Master of Science

(in Oceanography)

The Graduate School

The University of Maine

May 2017

Advisory Committee:

Emmanuel Boss, Ph.D., Professor of Oceanography, Advisor

Andrew Thomas, Ph.D., Professor of Oceanography

Mary-Jane Perry, Ph.D., Professor of Oceanography

© 2017 Nils Haëntjens
All Rights Reserved

REVISITING OCEAN COLOR ALGORITHMS FOR CHLOROPHYLL *A* AND PARTICULATE ORGANIC CARBON IN THE SOUTHERN OCEAN USING BIOGEOCHEMICAL FLOATS

By Nils Haëntjens

Thesis Advisor: Dr. Emmanuel Boss

An Abstract of the Thesis Presented
in Partial Fulfillment of the Requirements for the
Degree of Master of Science
(in Oceanography)
May 2017

The Southern Ocean (SO, oceans south of 30 °S) ecosystem plays a key role in global carbon cycles by sinking a major part (43 %) of the anthropogenic CO_2, and being an important source of nutrients for primary producers. However, undersampling of SO biogeochemical properties limits our understanding of the mechanisms taking place in this remote area. The Southern Ocean Carbon and Climate Observing and Modeling project (SOCCOM) has been deploying a large number of autonomous biogeochemical floats to study the SO (as of December 2016, 74 floats out of 200 have been deployed). SOCCOM floats measurements can be used to extend remote sensing chla and POC products under the clouds or during the polar night as well as adding the depth dimension to the satellites view of the SO.

Chlorophyll *a* (chla) concentrations measured by fluorometers (exciting/detecting light at 470/685 nm) embedded on the floats and particulate organic carbon (POC) concentrations derived from backscattering coefficients (at 700 nm) were calibrated with samples collected during the floats' deployment cruise. Float chla and POC were compared with products derived from observations of the Moderate Resolution Imaging Spectroradiometer *Aqua* (MODIS) and the Visible Infrared Imaging Radioneter Suite (VIIRS) sensors.

We find the Ocean Color Index (OCI) global algorithm to agree well with the matchups (within 9 %, on average, for VIIRS and 12 %, on average, for MODIS). SO specific algorithms estimating chla are offset by ∼45 % south of the Sea Ice Extent Front (∼ 60 °S). The remote sensing POC algorithm currently used by NASA agrees well with the float estimates throughout the SO.

REVISITING OCEAN COLOR ALGORITHMS FOR CHLOROPHYLL *A* AND PARTICULATE ORGANIC CARBON IN THE SOUTHERN OCEAN USING BIOGEOCHEMICAL FLOATS

By Nils Haëntjens

Thesis Advisor: Dr. Emmanuel Boss

A Lay Abstract of the Thesis Presented
in Partial Fulfillment of the Requirements for the
Degree of Master of Science
(in Oceanography)
May 2017

Keywords: chlorophyll *a*, particulate organic carbon, biogeochemical floats, southern ocean, ocean color

The Southern Ocean, defined as the oceans south of 30 °S, plays a key role in ocean acidification, in fact, it absorbs 43 % of the carbon dioxide emissions from human soll *a*urces (the major being electricity production, heat production, and transportation). However, our understanding of the biological (plankton) and chemical processes taking place in this remote region of the ocean is limited by the few samples collected to date. In order to unlock the mysteries of this ocean and improve our knowledge on the impacts of climate change, the Southern Ocean Carbon and Climate Observing and Modelling project (SOCCOM) has been deploying many robotic platforms able to profile the ocean from the surface to

2000 m deep equipped with advance sensors (temperature, salinity, nitrate, pH, oxygen, backscattered light, and fluorescence).

Chlorophyll *a* concentrations are retrieved from the fluorescence sensor, particulate organic carbon (POC) is derived from the backscattering signal. Both products tell us about the biomass and the physiological state of phytoplankton, which play a key role in the carbon cycle. Phytoplankton absorb (fix) CO_2 and produce O_2. When they are eaten, some of the carbon they fixed sinks to depth, and that way the Southern Ocean acts as a net sink for CO_2. The sensors are calibrated with water samples collected during their deployment. The float chlorophyll *a* and POC concentrations are compared with satellite observations for inter-calibration purposes.

We find that the global algorithm used by default on satellites, named the Ocean Color Index (OCI), agrees well (within 12 %) with the float chlorophyll *a* concentrations. Southern Ocean specific algorithms are offset by ∼45 % south of the Sea Ice Extent Front (∼ 60 °S). The POC algorithm currently used by NASA agrees well with the floats estimates throughout the SO.

ACKNOWLEDGEMENTS

I would first like to thank my advisor Emmanuel Boss, as well as my committee members Andrew Thomas and Mary Jane Perry to keep me in the right direction whenever needed and for the tremendous amount of ideas they provided to enrich this work. I would like to thank my family and friends for their continous support and encouragement, as well as, my office mates Lino Augusto Sander de Carvalho, Alison Chase, Jordan Snyder, and Nicholas DelPrete for the numerous tricks they provided easing the task, their valuable comments on this thesis, and the cheerfulness they brought in the office.

I would like to thank the SOCCOM community for their amazing work and for providing the dataset used in this study, as well as Stephen Riser and Ken Johnson for the pre-SOCCOM dataset, the many colleagues who helped with shipboard sampling, and analysis by SIO, CSIRO, UCSB, and NASA Ocean Biology and Biogeochemistry group. We thank Ryan Weatherbee for helping to process satellite imagery and useful comments from Magdalena Carranza and Sarah Gille. We also thank Dana Swift for integration of optical sensors and dark values measurement, as well as, Mati Kahru and Greg B. Mitchell for their help with SPGANT and their expertise of remote sensing in the SO.

SOCCOM is supported by the National Science Foundation (NSF), Division of Polar Programs under NSF Award PLR-1425989, with additional support from NOAA US Argo program supplying profiling floats, and NASA grant NNX14AP49G supplying bio-optical sensors for the pre-SOCCOM and SOCCOM floats. Logistical support for this project in Antarctica was provided by the U.S. National Science Foundation through the U.S. Antarctic Program. We acknowledge NASA Goddard Space Flight Center, Ocean Ecology Laboratory, and

Ocean Biology Processing Group for making and sharing Ocean Color data from MODIS and VIIRS Reprocessing 2014.0 [*NASA Goddard Space Flight Center*, 2014, 2015].

TABLE OF CONTENTS

LIST OF TABLES

LIST OF FIGURES

Chapter 1
INTRODUCTION

The Southern Ocean (SO), the oceanic region between 30 °S and Antarctica, occupies 30 % of the world's oceans, but plays a disproportionate role in their biogeochemistry: 43 % of anthropogenic CO_2 is taken up in the SO [*Frölicher et al.*, 2015] and it is the source of 75 % of nutrients used by primary producers north of 30 °S [*Sarmiento et al.*, 2004]. In realization of its contributions and in light of the lack of year-round data, a consortium of scientists has built a profiling-float based observatory equipped with state-of-the-art biogeochemical sensors.

The Southern Ocean Carbon and Climate Observations and Modeling (SOCCOM) is a six-year NSF-funded initiative that received additional funding from NOAA and NASA. SOCCOM floats, deployed in the SO, are typically equipped with CTD, nitrate, oxygen, and pH sensors, as well as sensors that measure light backscattered at 700 nm and chlorophyll *a* (chla) fluorescence. The latter provides an opportunity to validate space-derived biogeochemical products from another spatially and temporally extensive observation system, Ocean Color (OC). While much of the SO can be observed by OC year around, the regions south of 55 °S are not observed for several months of the year due to either low sun angle or absence of sunlight [*Behrenfeld et al.*, 2016].

Since the launch of NASA's Coastal Zone Color Scanner (CZCS), OC has been used to derive biogeochemical parameters in the SO, in particular chla and particulate organic carbon (POC). It has been found, however, that in the SO the globally derived empirical chla algorithms are biased. *Mitchell and Holm-Hansen* [1991], and *Sullivan et al.* [1993] found a significant (factor of 2.4) underestimate of

SO chla by the global CZCS algorithm. *Dierssen and Smith* [2000], found a similar bias (factor of ~ 2) with the Sea-Viewing Wide Field-of-View Sensor's (SeaWiFS) algorithm. These studies were based on a large database of fluorometrically extracted chla. *Mitchell and Kahru* [2009] and *Kahru and Mitchell* [2010] proposed an algorithm (SPGANT) for the Advanced Earth Observing Satellite (ADEOS), SeaWiFS, and the Moderate Resolution Imaging Spectroradiometer *Aqua* (MODIS) satellites, to correct this SO bias. *Guinet et al.* [2013] have found, using chla fluorometers mounted on elephant seals calibrated with High Performance Liquid Chromatography (HPLC), a bias of ~ 2 with MODIS. Finally, *Johnson et al.* [2013], have found using a large HPLC-based chla dataset (~ 1400 samples) that NASA's SeaWiFS and MODIS algorithms underestimated chla by a factor of about 3 and 4, respectively, at latitudes south of 35 °S and between 20-160 °E. Species composition, physiology and particulate composition were invoked to explain this under-estimation [see review of *Dierssen*, 2010]. Note, however, that *Marrari et al.* [2006] observed no significant bias between SeaWiFS' chla and HPLC chla.

The remoteness of the SO and the limited ability to cover its extent with research expeditions, have limited the exercise of satellite and *in situ* matchups to selected regions and seasons. For example, the bulk (> 95 %) of the data in *Johnson et al.* [2013] was collected in a narrow corridor south of Tasmania, located between 140-150 °E. In *Mitchell and Kahru* [2009], the *in situ* data was collected from 1997 to 2008, primarily in summer and in the Scotia Sea. *Guinet et al.* [2013] covered several seasons (December 2007 to February 2011) but were limited to the region south of the Indian Ocean. Wide areas such as the south Pacific Ocean and the southeastern Atlantic Ocean had no matchups in those studies.

Here, we use a recently assembled HPLC and POC dataset, collected in conjunction with SOCCOM profiling float deployments on 5 different SO cruises,

to evaluate the performance of NASA's MODIS and Visible Infrared Imaging Radioneter Suite (VIIRS) global algorithms. MODIS and VIIRS are polar orbitting multispectral satellites with visible and infrared detectors to measure top of the atmosphere (TOA) radiance. The products used are derived from the TOA radiance by applying an atmospheric correction [*Mobley et al.*, 2016] and application of community developed algorithms by the NASA Ocean Biology and Biogeochemistry group. *In situ* HPLC and POC data are used to calibrate sensors (chla fluorescence and scattering around an angle in the back direction) deployed on profiling floats [Johnson et al. 2017, submitted]. These calibrated sensors, in turn, are used to assemble a float-OC matchup dataset throughout the SO. With this dataset we find no statistically significant bias of NASA's MODIS and VIIRS algorithms for both chla or POC.

Chapter 2
METHODS

2.1 Sampling from the Cruises and Method of Analysis

Calibration of the optical sensors mounted on the floats is done by regressing the dark-adjusted, non-photochemical quenching (NPQ) corrected, and factory calibrated measurements of chlorophyll *a* (chla) and particulate backscattering (bbp) at 700 nm with biogeochemical analysis performed on water collected from the research vessels casts performed during deployment of the floats. *In situ* measurements were made within 24 hours of deployment (see locations on Figure 2.1). These calibration data are available from the five deployment cruises (Table 2.1) further detailled in Lynne et al. [2017], submitted. Water samples were collected with the CTD rosette at several depths and a volume of 1 or 2 L was filtered on glass fiber filters (GFF) shortly after collection and then stored in liquid nitrogen. The filters for high performance liquid chromatography pigment analysis (HPLC) were shipped and analysed at NASA GSFC (except for the SOTS cruise which was analysed at CSIRO following the same protocol) and for particulate organic carbon (POC) to UCSB.

The HPLC analysis follows the protocol of *Van Heukelem and Thomas* [2001] [further described in *Hooker et al.*, 2005] and is recognised by a general consensus

Table 2.1. List of cruises during which HPLC and POC samples were collected and used to calibrate floats sensors. More informations on the cruises are available in Talley et al. [2017] (submitted).

Cruise	Expedition code	# HPLC samples	# POC samples	# Float deployed	Latitude Range	Longitude Range	Sampling Period
P16S	320620140320	80	61	12	67 °S to 15 °S	174 °E to 149 °W	Mar-May 2014
A12	06AQ20141202	37	38	12	70 °S to 37 °S	9 °W to 13 °E	Dec 2014-Jan 2015
SOTS	096U20150321	0	14	1	47 °S to 46 °S	141 °E to 144 °E	Mar 2015
OOISO	320620151206	4	4	3	54 °S to 53 °S	89 °W to 80 °W	Dec 2015
P15S	096U20160426	20	20	10	66 °S to 46 °S	171 °W to 169 °W	May 2016

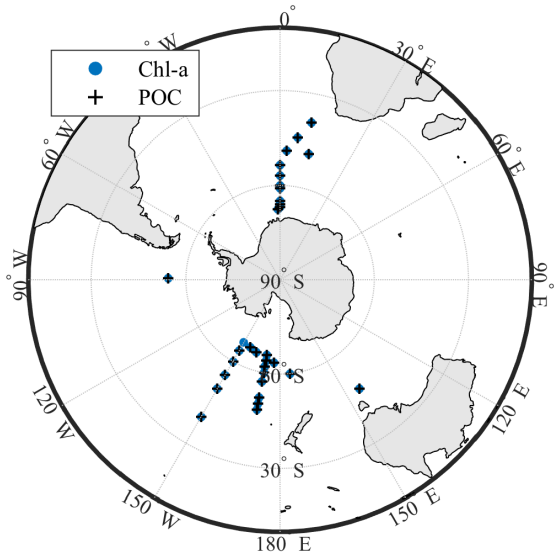

Figure 2.1. Map of matchups between water samples (for POC or HPLC analysis) and the first profiles of the SOCCOM and pre-SOCCOM floats.

[*Hooker et al.*, 2009] to be the most accurate method to measure [chla] in addition to providing the concentration of several accessory pigments. The total [chla] reported from HPLC corresponds to the sum of divinyl chlorophyll *a*, monovinyl chlorophyll *a*, chlorophyllide *a*, chlorophyll *a* allomers, and chlorophyll *a* epimers. The POC samples are acidified to get rid of inorganic carbon. A dry blank (unused filter), is collected at the time of sampling to account for potential contamination between the time at which the sample was taken and analysis in the lab. The POC extracted from the dry blank was removed from the POC extracted for each sample. Unfortunately, a "wet" blank filter to account for the effect of dissolved organic carbon (DOC) adsorption was not taken. For the volume filtered for this work, such blanks typically vary between 20-40 mgC m^{-3} [Cetinić, 2016, personal communication] and contribute to an unknown positive bias here.

2.2 Parameters Measured by Floats

Pre-SOCCOM and SOCCOM float profiles from the FloatViz archival dataset of November 28, 2016, are used in this study (Table 2.2). Optical data is collected on the float using one of two models of bio-optical sensors: the WET Labs ECO-FLBB with a chla fluorometer (EX/EM 470/695 nm) and backscatter (700 nm, centroid scattering angle, $\theta = 142°$) which are mounted on the majority of the floats, or the WET Labs MCOMS, present on few floats, which includes a chla fluorometer (EX/EM 470/695 nm), a backscatterer (700 nm, $\theta = 150°$) and a CDOM fluorometer (EX/EM 370/460 nm). The only difference is the angle of scattering in the back-direction. Everything else discussed here pertains to both sensors. A review of the WETLabs sensor performance and issues was recently published *Sullivan et al.* [2013]. To check for sensors drift we looked at the signal at 1000 m and found them to vary by 2 to 3 counts (except a few spikes) within the lifetime of a float. The order of variability is close to the sensitivity limit of the instruments (~ 1.4 counts for fluorescence and ~ 1.8 counts for backscattering).

2.3 Processing Float Measurements

2.3.1 Chlorophyll *a* Fluorescence

The concentration of chlorphyll *a* is initially estimated from the fluorescence signal using the linear relation provided by the manufacturer (eq. 2.1).

$$[chla] = slope \times (signal - dark) \tag{2.1}$$

Often the factory dark value does not represent the dark value in the field well due to differences in the platform on which it is measured and to fluorescence by dissolved organic material (FDOM). We use a modified version of the minimum offset method of *Xing et al.* [2017] namely estimating the dark based on the

Table 2.2. List of the 50 floats and associated bio-optical sensor from the FloatViz archival dataset of November 28, 2016. The oceanic zones are shown on the map Figure 2.4 and their acronyms stands for: sea ice zone (SIZ), Polar Antarctic Zone (PAZ), Subantarctic Zone (SAZ), and the Subtropical Zone (STZ)

UW Id[a]	WMO Id[b]	Sensor Model	Sensor SN	# Profiles	Zone	Date First Profile	Date Last Profile
0037	5904475	MCOMS	0015	79	STZ	05-Dec-2014 21:51:00	26-Nov-2016 00:33:00
0068	5903717	FLBBAP2	1550	243	SAZ, SIZ	19-Feb-2012 08:08:00	31-May-2016 03:24:00
0506	5904670	MCOMS	0109	8	SIZ	24-Jan-2016 08:24:00	03-Apr-2016 15:06:00
0507	5904671	MCOMS	0114	29	SIZ	15-Feb-2016 15:53:00	22-Nov-2016 01:25:00
0508	5904476	MCOMS	0032	54	SAZ, PAZ	09-Dec-2014 14:17:00	29-Feb-2016 04:35:00
0509	5904477	MCOMS	0017	17	PAZ, SIZ	13-Dec-2014 01:11:00	02-Jun-2015 06:56:00
0510	5904686	MCOMS	0115	27	PAZ, SIZ	25-Feb-2016 15:45:00	22-Nov-2016 19:52:00
0511	5904478	MCOMS	0034	4	SIZ	18-Dec-2014 16:32:00	17-Jan-2015 20:15:00
0564	5904687	MCOMS	0113	8	SIZ	23-Feb-2016 12:39:00	02-May-2016 20:49:00
0566	5904766	MCOMS	0118	20	PAZ	16-May-2016 04:29:00	22-Nov-2016 04:11:00
0571	5904673	MCOMS	0059	20	PAZ	12-May-2016 17:42:00	19-Nov-2016 03:41:00
6091	5904179	FLBB	3144	95	SAZ, PAZ	27-Mar-2014 05:11:00	20-Nov-2016 23:51:00
6967	5903612	FLBBAP2	2100	221	STZ, SAZ	11-Dec-2011 22:53:00	21-Feb-2016 17:08:00
6968	5903718	FLBBAP2	1738	250	SAZ	06-Mar-2012 01:44:00	21-Sep-2015 12:05:00
7552	5903593	FLBBAP2	1890	250	STZ, SAZ	15-Mar-2012 03:35:00	28-Oct-2015 08:56:00
7557	5904181	FLBB	3146	15	SAZ	28-Mar-2014 18:30:00	19-Aug-2014 21:06:00
7567	5904182	FLBB	3145	38	SAZ	10-Apr-2014 06:06:00	26-Apr-2015 19:15:00
7613	5904180	FLBB	3148	78	SAZ	31-Mar-2014 19:35:00	31-May-2016 12:56:00
7614	5904183	FLBB	3147	75	SAZ	01-Apr-2014 17:04:00	02-May-2016 10:04:00
7619	5904105	FLBBAP2	1887	182	SAZ, PAZ, SIZ	03-Mar-2013 07:22:00	15-Aug-2016 23:24:00
7620	5904104	FLBBAP2	1888	207	SAZ, PAZ, SIZ	04-Mar-2013 12:57:00	24-Nov-2016 16:54:00
7652	5904467	FLBB	3291	53	SAZ, SIZ	14-Dec-2014 19:03:00	02-Jun-2016 01:09:00
8514	5904470	FLBB	2993	67	SAZ	26-Mar-2015 20:17:00	23-Nov-2016 14:00:00
9031	5904396	FLBB	3306	129	SAZ	12-Apr-2014 03:35:00	03-Nov-2016 23:27:00
9091	5904184	FLBB	3308	95	SAZ	03-Apr-2014 23:12:00	27-Nov-2016 09:22:00
9092	5904185	FLBB	3173	94	SAZ	07-Apr-2014 23:03:00	22-Nov-2016 21:07:00
9094	5904471	FLBB	3641	51	SAZ, SIZ	21-Dec-2014 12:49:00	30-May-2016 20:27:00
9095	5904188	FLBB	3307	114	SAZ	15-Apr-2014 07:13:00	26-Nov-2016 09:40:00
9096	5904469	FLBB	3327	70	SAZ, PAZ	11-Dec-2014 12:34:00	23-Nov-2016 09:05:00
9099	5904468	FLBB	3178	49	SIZ	19-Jan-2015 22:11:00	28-May-2016 15:19:00
9125	5904397	FLBB	3309	49	SAZ, SIZ	22-Jan-2015 05:31:00	31-May-2016 01:16:00
9254	5904395	FLBB	2935	131	SAZ	21-Apr-2014 18:56:00	26-Nov-2016 02:01:00
9260	5904473	FLBB	3640	64	SAZ, PAZ	28-Jan-2015 07:05:00	09-Nov-2016 11:13:00
9275	5904472	FLBB	3643	42	SAZ	18-Jan-2015 21:56:00	27-Mar-2016 07:10:00
9313	5904474	FLBB	3646	87	STZ, SAZ, PAZ	07-Dec-2014 23:50:00	24-Nov-2016 04:15:00
9600	5904688	FLBB	3811	26	STZ, SAZ	06-Mar-2016 01:45:00	19-Nov-2016 16:29:00
9602	5904684	FLBB	3655	25	PAZ	28-Feb-2016 22:15:00	17-Nov-2016 18:51:00
9631	5904677	FLBB	3686	28	SAZ, PAZ	01-Apr-2016 17:22:00	25-Nov-2016 00:24:00
9632	5904763	FLBB	3682	19	SAZ	19-May-2016 10:24:00	20-Nov-2016 13:06:00
9634	5904693	FLBB	3809	19	SAZ	20-May-2016 18:33:00	23-Nov-2016 06:08:00
9637	5904682	FLBB	3810	27	SAZ, PAZ	02-Mar-2016 03:24:00	26-Nov-2016 21:28:00
9645	5904676	FLBB	3688	29	SAZ, PAZ	18-Jan-2016 05:38:00	20-Nov-2016 18:14:00
9646	5904661	FLBB	3806	33	SAZ	29-Dec-2015 05:25:00	24-Nov-2016 22:22:00
9650	5904683	FLBB	3685	27	SAZ, PAZ	03-Mar-2016 23:57:00	28-Nov-2016 00:56:00
9652	5904660	FLBB	3803	32	SAZ	07-Jan-2016 19:29:00	24-Nov-2016 09:31:00
9657	5904659	FLBB	3808	32	SAZ	08-Jan-2016 09:14:00	24-Nov-2016 02:37:00
9660	5904761	FLBB	3807	19	SAZ	18-May-2016 06:02:00	19-Nov-2016 17:01:00
9744	5904678	FLBB	3645	29	SAZ	07-Apr-2016 22:47:00	21-Nov-2016 11:36:00
9757	5904679	FLBB	3684	31	PAZ	19-Jan-2016 04:04:00	25-Nov-2016 16:46:00
9762	5904765	FLBB	3804	18	SAZ	31-May-2016 20:49:00	23-Nov-2016 20:02:00

[a]University of Washington identification number, used in FloatViz

[b]World Meteorological Organization identification number

minimum value of the fluorescence signal. A darkprofile is estimated as the median of the lowest values within a profile. It is calculated for all the profiles of a float over its lifetime (in delayed mode). The "global" minimum of all the darkprofile is the final chlorophyll dark of the float. Compared with the manufacturer dark we find that the error induced represents, on average, about 1 % of the signal (and hence chla) in the mixed-layer (equivalent to 0.01 mg m^{-3}). Phytoplankton require light for photosynthesis; however, too much light can lead to pigment bleaching or death. To protect their photosystems from high light intensity algae regulate the absorption and utilisation of light energy. This photo-protection mechanism, known as non-photochemical quenching (NPQ), induces an important decrease in the fluorescence to [chl-a] ratio (*Kolber and Falkowski* [1993]; *Muller et al.* [2001]). Some of the float profiles are done during daylight, resulting in NPQ of the measured fluorescence. To determine if a profile is quenched or not we estimate the sun elevation angle from *Reda and Andreas* [2004]. The chla fluorescence profile is corrected for NPQ if the sunelevation $> 5°$ using the average of two correction methods: (1) *Sackmann et al.* [2008] use the backscattering channel, and (2) *Xing et al.* [2012] who assume a constant [chla] above the mixed layer depth (MLD). The MLD used for these corrections was estimated with a fixed density threshold criterion of 0.005 kg m^{-3} which corresponds to a daily MLD (*Brainerd and Gregg* [1995]). We initially use the manufacturer calibration to convert the sensor output into estimates of chla concentration, as WETLabs cross-calibrates all its sensors. A vicarious calibration is conducted by regressing the estimated chla of the first profile of the float and the matching total chla concentration estimated with HPLC taken close to the float deployment. This second calibration provide the factors used to convert the float measurements to chla (Figure 2.2). We conducted both a linear and a non-linear regression (both requiring only two parameters, table 2). The slope of the linear regression (6.4) is consistent with a recent analysis

Table 2.3. Regressions between the float measurements of chla (mg m^{-3}) or POC (mg m^{-3}) and discrete samples analysis (HPLC and POC).

Relationship	n	r^2	$RMSD$ (mg m^{-3})	$RMSRD$
$chla_{HPLC} = 0.15(\pm 0.017) \times chla_{float}$	73	0.77	0.20	0.48
$chla_{HPLC} = 0.213(\pm 0.016) \times chla_{float}^{0.714(\pm 0.242)}$	73	0.80	0.12	0.37
$POC = 3.12 \times 10^4(\pm 2.47 \times 10^3) \times b_{bp}(700) + 3.04(\pm 6.78)$	67	0.76	35	0.47
$POC = 9.776 \times 10^4(\pm 1.90 \times 10^4) \times b_{bp}(700)^{1.166(\pm 0.173)}$	67	0.88	40	0.59

of the relationship between fluorescence measured with WETLabs fluorometers and HPLC [Roesler et al. 2017, accepted]. We found the non-linear fit to perform significantly better (Table 2.3, 3.1) and used it subsequently.

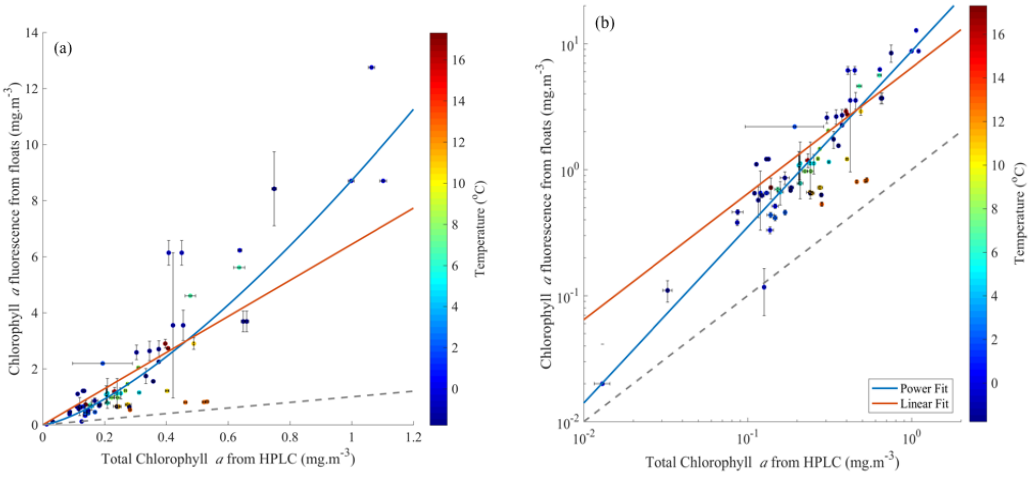

Figure 2.2. Relationship between total chlorophyll a (from HPLC) and chla fluorescence (from floats) adjusted for darks and corrected for NPQ on a linear scale (a) and log/log scale (b). The red line is a linear fit with a slope of 6.4 (Table 2.3), the blue line is a power law fit (Table 2.3), and the 1:1 relationship is the dashed grey line. Uncertainties of total chlorophyll a correspond to the standard deviation of all the replicates (if available). Uncertainties of the chlorophyll a fluorescence corresponds to the standard deviation of all the measurements taken by the float within 5 meters of the sampling depth.

2.3.2 Particulate Organic Carbon

We obtain the volume scattering function β from the raw signal:

$$\beta = slope \times (signal - dark) \tag{2.2}$$

The manufacturer slope factor and dark counts are used unless a pre-deployment dark is available. The backscattering coefficient of particles b_{bp} is commonly estimated from measurement of scattering at a single angle in the backward hemisphere $\beta(\theta)$ which is a function of the scattering angle θ (142° and 150° for FLBB and MCOMS respectively, all at 700 nm).

$$\beta_p(\theta) = \beta(\theta) - \beta_{sw}(\theta) \tag{2.3}$$

$$b_{bp} = 2 \times \pi \times \chi_p(\theta) \times \beta_p(\theta) \tag{2.4}$$

$\beta_{sw}(\theta)$ is the volume scattering function of sea water using local temperature and salinity and is estimated with the *Zhang et al.* [2009] algorithm and $\chi_p(\theta)$ is the particulate conversion coefficient from *Sullivan et al.* [2013]. An empirical relationship between particulate backscattering at 700 nm and POC for the SOCCOM floats is done by regressing the POC samples with the bbp estimated from the first profile the floats. The regression found (Table 2.3, Figure 2.3) is consistent with the literature [*Cetinić et al.*, 2012].

2.3.3 Uncertainties Associated with Float Products

2.3.3.1 Chlorophyll *a* Uncertainties

Chlorophyll *a* concentrations estimated from the fluorometers are limited by the sensitivity of the instrument which is consistent between floats and is on average $\Delta_{res} = \sim 0.003$ mg m^{-3} for the MCOMS and ~ 0.007 mg m^{-3} for the FLBB. The uncertainty associated with the dark correction multiplies this uncertainty by $\sqrt{2}$, assuming they are uncorrelated. The relative error associated with the adjustment of the chla values with the HPLC is estimated with the standard deviation of the slope (Table 2.3) and represents $\epsilon_{slope} = 11$ % of the signal. If a NPQ correction was needed, the corresponding uncertainty defined by ΔNPQ is added to the total

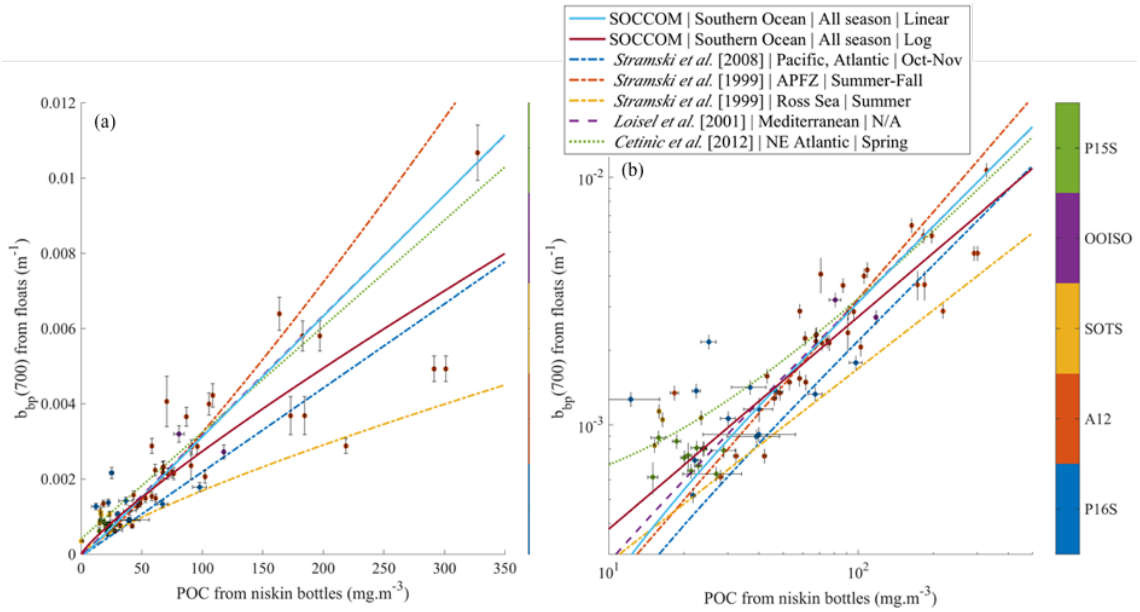

Figure 2.3. Relationship between POC (from discrete samples taken in the upper 100 m during float deployment) and bbp(700) on the first float profile on linear scale (a) and log/log scale (b). bbp(700) from the floats are averaged in the 5 meters around the depth at which water samples are taken. Equations reported in other studies are shown as dashed lines. Uncertainties are estimated with the same method as in Figure 2.2

uncertainty.

$$\Delta_{NPQ} = chla_{NPQ_{X12}} - chla_{NPQ_{S08}} \tag{2.5}$$

with $chla_{NPQ_{X12}}$ and $chla_{NPQ_{S08}}$ as the signal corrected for NPQ with *Xing et al.* [2012] and *Sackmann et al.* [2008], respectively. We assume no correlation between the uncertainties, thereafter the total uncertainty Δ_{chla} is:

$$\Delta_{chla} = \sqrt{max(\sqrt{2}\Delta_{res}, \epsilon_{slope})^2 + \Delta_{NPQ}^2} \tag{2.6}$$

The average relative error above max(Z_{MLD}, Z_{eu}) is 0.012 mg m^{-3} where the average absolute error is 0.01 mg m^{-3} for profiles not corrected for NPQ and 0.16 mg m^{-3} if profiles are corrected for NPQ.

2.3.3.2 POC Uncertainties

Uncertainties associated with particulate backscattering (Δ_{bbp}) are due to instrument sensitivity and methodological uncertainties.

$$\Delta_{b_{bp}} = max(\sqrt{\Delta_{res}^2 + \Delta_{dark}^2}, \epsilon_{\beta_{sw}}) \tag{2.7}$$

Average instrument resolution of SOCCOM floats is $\Delta_{res} = 5.8 \times 10^{-7}$ for MCOMS and $\Delta_{res} = 2.1 \times 10^{-6}$ for FLBB. The uncertainty associated with the darks (Δ_{dark}) represents on average 1.11×10^{-5} m^{-1} (3 % of the signal near the surface and 11 % at depth). The relative error associated with the angular scatterance of seawater ($\epsilon_{\beta_{sw}}$) is 2 % [*Zhang et al.*, 2009]. Assuming no correlation between the errors of particulate backscattering, we estimate the average uncertainty as 5 % in max(Z_{MLD}, Z_{eu}) and 13 % near the parking depth, whereas *Boss and Pegau* [2001] estimate it to < 10 %. Uncertainty associated with the relationship between POC and bbp needs to be added to the POC product; the standard deviation of the slope and of the y-intercept found in Table 2.3 are used and represent about 8 % of the signal.

$$\Delta_{POC} = max(\sqrt{\Delta_{b_{bp}}^2 + \Delta_{POC}^2}, \epsilon_{b_{bp}} + \epsilon_{POC}) \tag{2.8}$$

The average absolute error is 9.62 mg m^{-3} and an average relative error of 3.74 mg m^{-3} above the max(Z_{MLD}, Z_{eu}), which is very close to other local studies ~ 20 % using similar sensors [*Cetinić et al.*, 2012]. This relationship between POC and $b_{bp}(700)$ is derived for surface samples and is likely to be biased at depth below max(Z_{MLD}, Z_{eu}) and/or if inorganic sediments are in the water (e.g. river inflow, bottom re-suspension).

2.4 Comparison with Remote Sensing

Chla and POC are derived from remote sensing reflectance (R_{rs}) for both MODIS and VIIRS sensors reprocessing 2014.0 [*NASA Goddard Space Flight Center*, 2014,

2015]. The matchups with float profiles are broadly distributed around Antarctica, mainly south of 45 °S as presented in Figure 2.4, and cover multiple seasonal cycles.

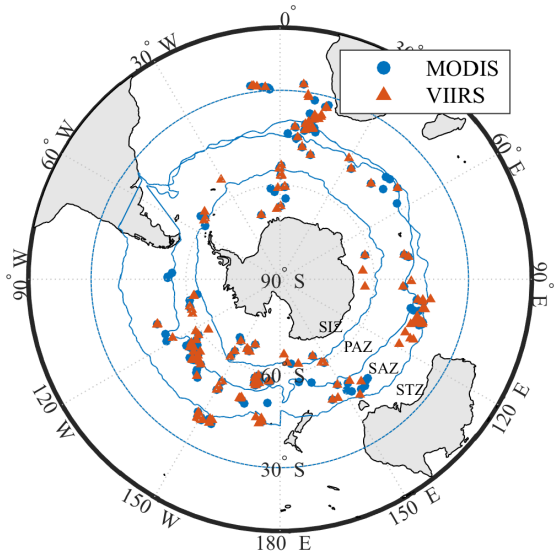

Figure 2.4. SOCCOM and pre-SOCCOM float and ocean color (OC) matchup locations (MODIS in blue circles and VIIRS in red triangles). The acronyms of each region of the Southern Ocean stands for: sea ice zone (SIZ), Polar Antarctic Zone (PAZ), Subantarctic Zone (SAZ), and the Subtropical Zone (STZ)

Ocean Color Index (OCI) [*Hu et al.*, 2012], the latest global inversion algorithm from NASA for chla, is compared to two algorithms specific to the Southern Ocean: SPGANT version 4 [*Kahru and Mitchell*, 2010; *Mitchell and Kahru*, 2009] and *Johnson et al.* [2013] (referred as J13, implementation in Table 2.4) as referred against chla estimated by floats. OCI is a blend of the band ratio algorithm OCx (OC3M or OC3V, for MODIS and VIIRS respectively) and the color index (CI) algorithm of *Hu et al.* [2012]; the algorithm transitions between $0.15 < [chla] < 0.20$ mg m^{-3}. This algorithm was not used as a default OC algorithm at the time at which SPGANTv4 and J13 were built. SPGANTv4 [*Mitchell and Kahru*, 2009] is used in conjunction with OC3M: for $[chla] <= 0.07$

Table 2.4. Inversion Algorithms

Product	Sensor	Algorithm	Equations
chla	MODIS	OCI[a]	Merged OC3M band ratio algorithm with color index (CI) of *Hu et al.* [2012]
chla	MODIS	J13[b]	$R_{sw} = log_{10}\left(\frac{max(R_{rs}(443),R_{rs}(488))}{R_{rs}(547)}\right)$ $chla_{J13} = 10^{0.6994-2.0384R_{sw}-0.4656R_{sw}^2+0.4337R_{sw}^3}$
chla	MODIS	SPGANTv4[c]	$L_{wn}(\lambda) = \frac{F_0(\lambda)\times R_{rs}(\lambda)}{\pi}$ $R = log_{10}\left(\frac{max(L_{wn}(443),L_{wn}(488))}{L_{wn}(547)}\right)$ $chla_{SPGANTv4} = 10^{0.5514-2.2434R+0.0746R^2-0.0095R^3-0.7790R^4}$ blended with OC3M [*Kahru and Mitchell*, 2010]
chla	VIIRS	OCI[a]	Merged OC3V band ratio algorithm with color index (CI) of *Hu et al.* [2012]
chla	VIIRS	J13[b]	$R_{sw} = log_{10}\left(\frac{max(R_{rs}(410),R_{rs}(443),R_{rs}(486))}{R_{rs}(551)}\right)$ $chla_{J13} = 10^{0.6736-2.0714R_{sw}-0.4939R_{sw}^2+0.4756R_{sw}^3}$
POC	MODIS	S08[d]	$POC = 203 \times \left(\frac{R_{rs}(443)}{R_{rs}(547)}\right)^{-1.034}$
POC	VIIRS	S08[d]	$POC = 203 \times \left(\frac{R_{rs}(443)}{R_{rs}(551)}\right)^{-1.034}$

[a] *Hu et al.* [2012]
[b] *Johnson et al.* [2013]
[c] *Kahru and Mitchell* [2010]; *Mitchell and Kahru* [2009]
[d] *Stramski et al.* [2008]

OC3M is used, between $0.07 < [chla] < 0.13$ a linear transition between the two algorithms occurs, and for $[chla] >= 0.13$ SPGANTv4 is used [*Kahru and Mitchell*, 2010]. The algorithm of *Stramski et al.* [2008] is used for POC.

In order to maximize the quality of the comparison between floats and OC, "good quality" matchups are required. *Bailey and Werdell* [2006] defined there as: a narrow time window (+/- 3 hours) between *in situ* and satellite records, computed from the mean of a 5x5 pixel box centered on the *in situ* measurement, and a good atmospheric correction (mask pixels with level 2 flags). For our dataset, this resulted in only 4 matchups with MODIS products. Several factors might explain this: the floats' surface time is not synchronized with NASA satellites' overpasses, cloud coverage is high all year long in the Southern Ocean, the polar night, and high solar zenith angle (> 70 deg) during several months.

Widening the spatial and temporal window increases the number of matchups at the possible cost of quality, but as mentioned in the report from *IOCCG* [2011], optical data exhibits large spatial and temporal correlations making it useful for matching-up beyond the narrow window specified above. A spatial correlation analysis (Figure 2.5), shows that we can increase the number of matchups significantly with a relatively small decrease in correlation by averaging products within an 8 km radius circle and a 24 hour window, keeping the same level 2 flags criteria as the "good quality" matchups.

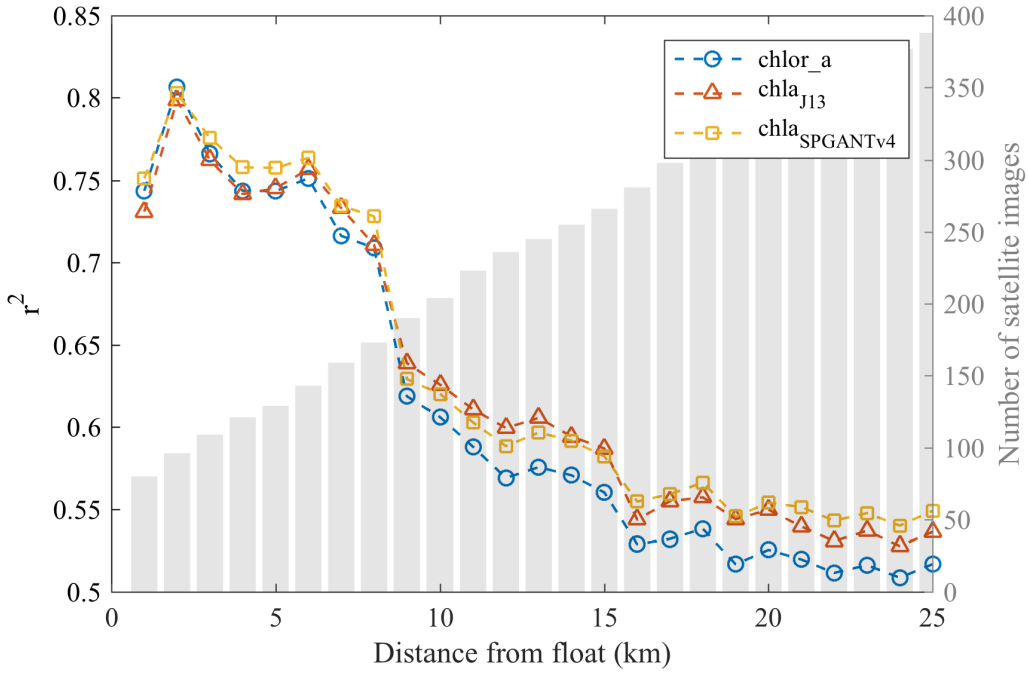

Figure 2.5. Spatial correlation between float and MODIS chlorophyll *a* (chla). The histogram represents the number of satellite images available, for a given radius around the position at which the float surfaced and within ±24 hours. The correlation coefficient (r^2) between float and MODIS chla vary as a function of the radius of the disk in which satellite pixels are averaged. Algorithms used to derive chla concentration from remote sensing reflectance are: OCI (chlor_a, blue circles), J13 ($chla_{J13}$, red triangles), and SPGANTv4 ($chla_{SPGANTv4}$, yellow squares). Similar results are observed with VIIRS.

To account for vertical structure of the water column, we optically weight chla and POC (eq. 2.9) from floats according to *Gordon and Clark* [1980] [*Mueller et al.*, 2003; *Werdell and Bailey*, 2005; *Zaneveld et al.*, 2005],

$$< chla >= \frac{\sum e^{-2K_d z} chla_{float}(z)}{\sum e^{-2K_d z}} \tag{2.9}$$

with K_d as the diffuse attenuation coefficient of downwelling irradiance at 490 nm, derived from satellite measurements (with KD2M and KD2V for MODIS and VIIRS respectively), and z as the depth.

2.4.1 Matchup Fits and Associated Statistics

Of primary interest is the slope of the linear type II regression [reduced major axis, defined by *Ricker*, 1973]. The regression's standard deviation (std) of both the slope and offset are computed following the treatment of *Ricker* [1973] for a model I regression. The squared Pearson's linear correlation coefficient (r^2) indicates the proportion of variance explained by a linear dependence between two independent variables, and is defined by:

$$\bar{x} = \frac{\sum_{i=1}^{n} x_i}{n} \qquad \bar{y} = \frac{\sum_{i=1}^{n} y_i}{n} \tag{2.10}$$

$$r^2 = \left(\frac{\sum_{i=1}^{n} (x_i - \bar{x})(y_i - \bar{y})}{\sqrt{\sum_{i=1}^{n} (x_i - \bar{x})^2 \times \sum_{i=1}^{n} (y_i - \bar{y})^2}} \right)^2 \tag{2.11}$$

with n as the number of matchups, x and y the two data sets (in our case, one is the product from the float (y) and the other is the product from the satellite (x)). The root mean square deviation ($RMSD$) was defined by:

$$RMSD = \sqrt{\frac{\sum_{i=1}^{n} (y_i - x_i)^2}{n}} \tag{2.12}$$

The root mean square relative deviation ($RMSRD$) is defined by:

$$RMSRD = \sqrt{\frac{\sum_{i=1}^{n} \left(\frac{y_i - x_i}{y_i} \right)^2}{n}} \tag{2.13}$$

The ratio from the RMSRD might be very large due to uncertainties in both float and OC datasets which bias the relative deviation. For this reason, a root mean square unbiased relative deviation (RMSURD) is also used, as defined by *Hu et al.* [2012]:

$$RMSURD = \sqrt{\frac{\sum_{i=1}^{n} \left(\frac{y_i - x_i}{0.5 \times (x_i + y_i)} \right)^2}{n}} \tag{2.14}$$

Chapter 3
RESULTS

We compare the float based estimates of chla and POC with those derived by remote sensing algorithms, using float and OC matchups. For chla concentrations we find that the global OCI algorithm performs better than the SO specific algorithms SPGANTv4 and J13 when all the regions are included (Table 3.1, Figure 3.1). In fact, the frequency distribution of the satellite data overlaps well with the frequency distribution of float observations (Figure 3.1, c and f). The OCI algorithm underestimates, on average, the [chla] by 9 % for VIIRS whereas it overestimates it by 12 % for MODIS. SPGANTv4 and J13 overestimate chla, on average, by a factor of 2 for all regions combined.

OCI's mean absolute deviation is on the order of 0.1 mg m^{-3} and is significantly lower (by a factor between 3 to 4) than J13 and SPGANTv4. The relative deviation exhibits the same trend. These metrics suggest that the OCI algorithm performs better than J13 and SPGANTv4 (Table 3.1). However, the unbiased relative deviation (RMSURD) between the float and OC chla of this study is higher ($\sim$ 45 %) than for the matchups used to build the relationship of the color index (CI) algorithm of *Hu et al.* [2012] (32.7 % for CI and 25.5 % for OC3M). The deviation from the *in situ* data (RMSD and RMSRD) for MODIS and VIIRS

Table 3.1. Regressions between the float measurements and satellite observations

Sensor	Algorithm	Slope Linear	Offset Linear mg m^{-3}	n	r^2 Linear	$RMSD$ Linear mg m^{-3}	$RMSRD$ Linear	$RMSURD$ Linear	r^2 Log	$RMSD$ Log mg m^{-3}	$RMSRD$ Log	$RMSURD$ Log
MODIS	OCI	0.88(±0.04)	0.01(±0.01)	173	0.67	0.11	0.73	0.45	0.58	0.21	1.55	0.40
MODIS	J13	0.35(±0.02)	0.07(±0.01)	173	0.66	0.43	1.74	0.74	0.60	0.36	5.59	342.00
MODIS	SPGANTv4	0.41(±0.02)	0.05(±0.01)	173	0.70	0.35	1.51	0.68	0.63	0.33	4.49	2.69
VIIRS	OCI	1.09(±0.05)	−0.02(±0.01)	203	0.61	0.10	0.61	0.44	0.50	0.20	0.73	0.44
VIIRS	J13	0.49(±0.03)	0.05(±0.01)	203	0.49	0.28	1.41	0.62	0.48	0.30	2.94	2.26
both	OCI	0.97(±0.03)	−0.00(±0.01)	376	0.63	0.10	0.67	0.45	0.54	0.20	1.18	0.43
MODIS	POC	0.94(±0.06)	−11.47(±5.08)	173	0.37	31.46	0.72	0.44	0.44	0.20	0.13	0.12
VIIRS	POC	1.15(±0.07)	−14.30(±5.41)	203	0.34	28.60	0.57	0.38	0.40	0.17	0.11	0.10
both	POC	1.05(±0.05)	−12.85(±3.79)	376	0.33	29.95	0.64	0.41	0.40	0.19	0.12	0.11

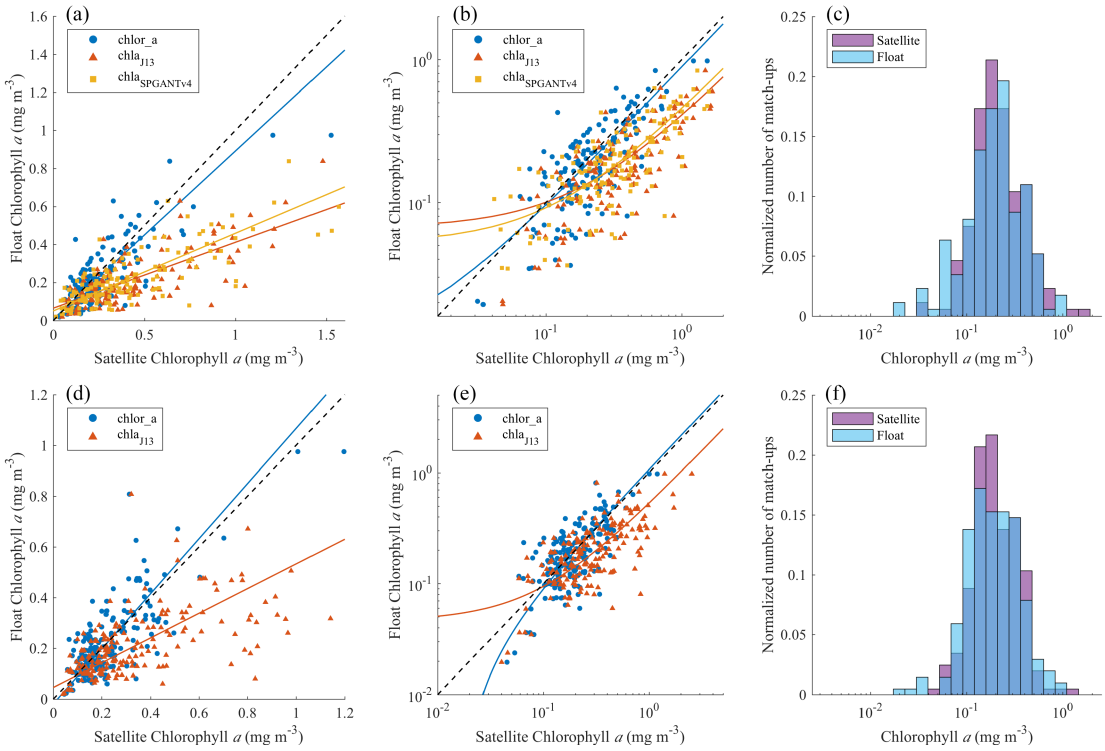

Figure 3.1. Chlorophyll a comparison in linear space (a, d) and log/log space (b ,e) of the following chlorophyll a inversion algorithms (Table 2.4): OCI (chlor_a, blue circles), J13 (chla$_{J13}$, red triangles), and SPGANTv4 (chla$_{SPGANTv4}$, yellow squares); for both MODIS (a, b, c) and VIIRS (d, e, f). The frequency distribution of the float (transparent blue) and OCI (purple) chlorophyll a concentration are presented in sub-figure (c) and (f). Statistics are presented in Table 3.1. Chlorophyll a from remote sensing is averaged within an 8 km radius circle.

sensors using J13 and SPGANTv4 algorithms was not reported in the relevant publications.

To study the biases, we analyze matchups as a function of the regions of the SO as defined by Gray et al. [2017] (submitted). The regions: Subantarctic Zone (SAZ), Polar Antarctic Zone (PAZ), south of the subtropical front (STF) and north of the mean 2014-2015 September sea ice extent, have a smaller slope (0.84 ± 0.10) , as opposed to the areas north and south of those boundaries, the Subtropical Zone (STZ) and the sea ice zone (SIZ), where the regression is 1.00 ± 0.10. However, for

the STZ, SAZ, and PAZ no significant offset is observed, whereas in the SIZ chla is underestimated ($\sim$ 20 %) by OCI (Figure 3.2, a). A similar study was conducted filtering the matchups by seasons, no significant bias or offset are observed for any season. During the winter no matchup are available in the SIZ and signficantly lower values are observed in the other regions.

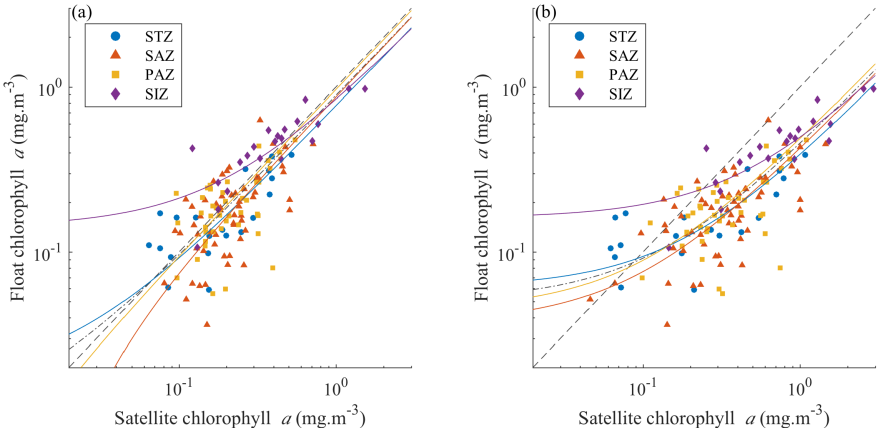

Figure 3.2. Regressions between float and MODIS chlorophyll *a* estimated with OCI (a) and SPGANTv4 (b) in log/log space. Solid lines correspond to the linear regressions by region: Sea Ice Zone (SIZ, purple diamonds), Polar Antarctic Zone (PAZ, yellow squares), Subantarctic Zone (SAZ, red triangles), and the Subtropical Zone (STZ, blue cicles). The 1:1 relationship is the dashed grey line and the linear regression for all regions combined is the gray dot-dash line.

Float-based POC estimates agree well with NASA's algorithm but also exhibit a large spread (relatively low prediction capability) in matchups (Table 3.1, Figure 3.3). The uncertainty of the POC for both sensors (Table 3.1) is very close to the one from the algorithm used [*Stramski et al.*, 2008] which has an RMSD = 21.3 mg m^{-3}, RMSRD = 21.7 %, r^2 = 0.87, for N = 53. This supports the consistency of this product across the globe and the SO.

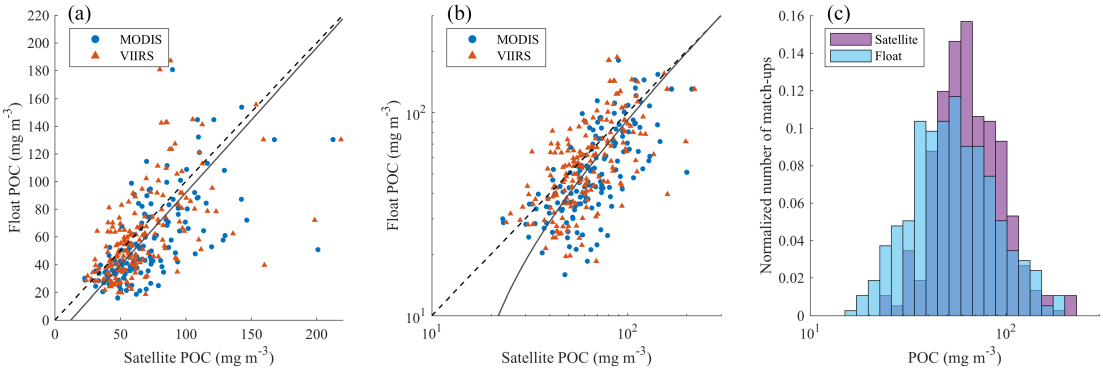

Figure 3.3. POC regressions between float and both satellite sensors (MODIS, blue circles; VIIRS, red triangles) using *Stramski et al.* [2008] (Table 2.4). (a) is in linear space, (b) is in log/log space, and (c) is an histogram of the frequency distribution of the data (satellite in purple and float in transparent blue). Statistics are presented in Table 3.1. POC from remote sensing is averaged within an 8 km radius circle.

Chapter 4
DISCUSSION

The comparison between OC and float POC (Figure 3.3) is likely biased, as our *in situ* POC measurements include some dissolved organic material (DOC) adsorbed by the filter which should result in an overestimation of the POC product estimated for the float. A recent analysis (Cetinić, personal communication 2016), suggests, for the amount of water filtered, a likely bias of 33 to 38 ($\pm$1.3) mg m^{-3}. On the other hand, frequency distributions of float POC overall underestimated the POC concentration (Figure 3.3, c), which is inconsistent with the above.

We find the SO-specific chla algorithms [*Johnson et al.*, 2013; *Kahru and Mitchell*, 2010; *Mitchell and Kahru*, 2009] overestimate [chla] concentration in the SIZ region where we expected them to perform better than OCI. The reason may be that the datasets used in the SO studies come from restricted seasons and regions in the SO, while our float-based dataset are spread wider geographically (South Pacific and South East Atlantic) and temporally (cover evenly over several seasonal cycles) in the SO (compare Figure 1 in *Johnson et al.* [2013] and Figure 2.4 in this paper). *Marrari et al.* [2006] compared chla from fluorometers calibrated with HPLC with chla from SeaWiFS estimated with OC4v4. They concluded that no significant bias was observed, which is similar to what we find here with MODIS and VIIRS. The dataset presented here shows small biases between regions of the SO, however more matchups are needed to properly address spatial and temporal biases. Those biases may be related to specific physiological state and species composition as the *IOCCG* [2015] report suggests.

In this analysis we assume the ratio of chla to fluorescence yield (fl) to be constant (Figure 3.1), however the variability is large in the world ocean [*Cullen*, 1982,

Roesler et al. 2017, submitted]. Phytoplankton acclimate to light intensity, nutrient concentrations, trace metals concentrations, and extremely cold temperatures [*Behrenfeld et al.*, 2005; *Cullen*, 2015; *Dierssen*, 2010] by changing their intercellular chla concentration and their fluorescence yield. In addition, this ratio also varies with species composition [*Proctor and Roesler*, 2010]. Fluctuations in the chla:fl ratio could, potentially, be modelled with parameters such as PAR, temperature, day of the year, and nutrient concentration in order to enhance our measurements of phytoplankton biomass with both autonomous platforms and satellites.

Non-photochemical quenching corrections [*Sackmann et al.*, 2008; *Xing et al.*, 2012] used to produce our dataset could introduce significant uncertainty in the chla concentration estimated from the fluorometers. However, we find that removing the NPQ corrected data from the relation used here changed the slope factor by less than 10 %, suggesting that NPQ does not bias the observed relationship. The quality of the relationships could potentially be improved by using mechanistic models (Xing et al. [2017], submitted) or by using a radiometer in addition to the chla fluorometer to compute chla [*Xing et al.*, 2011]. Such radiometers are recommended for BGC floats by *Johnson and Claustre* [2016].

An independent dataset of 6242 HPLC samples from 1682 profiles between Oct 1995 and April 2011 from NASA's SeaBASS database (all the data available on February 1, 2017, south of 30 °S) is compared to MODIS OCI matchups (no image available for VIIRS). Out of the 659 matchups only 97 respected the criteria we used here (Figure 4.1). The slope of the regression between the *in situ* and OCI chla is similar to the one obtained with the float comparison, which supports the relationship developped in Figure 3.1.

ll a

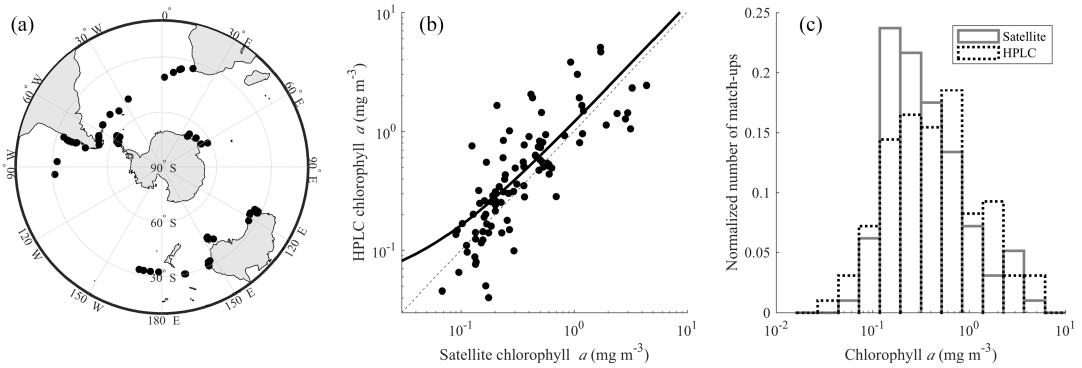

Figure 4.1. From left to right: map of area south of 30 °S(a), regression (b), and histogram (c) of the matchups between the SeaBASS database of *in situ* chlorophyll *a* from HPLC analysis and MODIS chlorophyll *a* from OCI on left. The regression plot is in log/log space, the dashed line correspond to the 1:1 line, the black line is a linear regression type II ($chla_{HPLC} = 1.15(\pm 0.11) \times chla_{sat} + 0.05(\pm 0.11)$. In linear space, RMSD = 0.78 mg m^{-3}, RMSRD = 0.70, RMSURD = 0.59, and N = 97.

To further validate our float dataset the ratio of chla to phytoplankton carbon (C_{phyto}) is compared to previous studies. C_{phyto} is computed with each method described in *Thomalla et al.* [2017] (except for the method B05 [*Behrenfeld et al.*, 2005], where $b_{bp}(440)$ is used instead of $b_{bp}(470)$). The shift in particulate backscattering wavelength is estimated with $b_{bp}(\lambda) = b_{bp}(700)\left(\frac{\lambda}{700}\right)^{-\gamma}$, with $\gamma = 0.78$ [*Boss et al.*, 2013]. A few negative concentrations of C_{phyto} computed with the M13 [*Martinez-Vicente et al.*, 2013] method are ignored. A time series of the ratio of chla:C_{phyto} corresponding to the average of all the measurements in the SAZ shallower than 25 m within a 10 day window is shown in Figure 4.2. The 5 seasonal cycles covered by the SOCCOM dataset allow visualization of the low light acclimation of phytoplankton (more chla per cell) and deep mixing layer during the winter (Figure 4.2). The data show that our trends are consistent with *Thomalla et al.* [2017], a general agreement with chla-based estimates [*Sathyendranath et al.*, 2009], a bias of ~ 2 for methods based on both

backscattering and chla, and that the chla:C_{phyto} are in the range specified by *Behrenfeld et al.* [2005] for the SO [except the ratio obtained with the method from *Sathyendranath et al.*, 2009]. To evaluate the correct chla:C_{phyto} further work is needed using methodology such as *Graff et al.* [2015] who measured C_{phyto} directly.

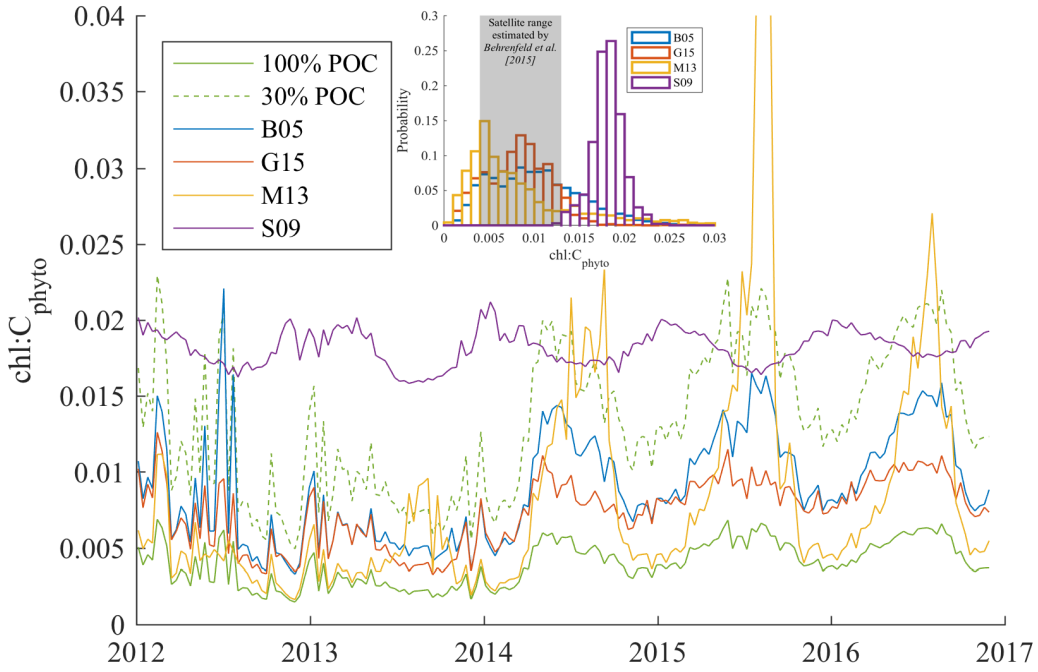

Figure 4.2. Time series of chlorophyll *a* to phytoplantkton carbon (C_{phyto}) ratio from all the SOCCOM and pre-SOCCOM floats in the Subantarctic Zone (SAZ). C_{phyto} is estimated with 6 different methods: 100 % POC (green) assume that [C_{phyto}] is 100 % of [POC]; 30 % of POC (dashed green) assume that [C_{phyto}] corresponds to 30 % of [POC] [following *Thomalla et al.*, 2017]; B05 (dark blue) estimates [C_{phyto}] based on $b_{bp}(440)$ with *Behrenfeld et al.* [2005]; G15 (red) estimates C_{phyto} based on $b_{bp}(470)$ with *Graff et al.* [2015]; M13 (yellow) estimates [C_{phyto}] based on $b_{bp}(470)$ with *Martinez-Vicente et al.* [2013]; S09 (purple) C_{phyto} based on [chla] with *Sathyendranath et al.* [2009]. The range of chla:C_{phyto} ratio retrieved from remote sensing for the Southern Ocean, 0.004 to 0.013 [*Behrenfeld et al.*, 2005], is displayed as a gray area on the frequency distribution diagram of the data. The peak of chl:C_{phyto} estimated with M13 in August 2015 reach its maximum at 0.054. Note that the number of measurements is limited during 2012 and 2013.

Chapter 5
CONCLUSION

Our results support the use of the OCI algorithm in the SO. OCI, the default algorithm to estimate chla from NASA, performs well in the SO (average bias of 9 % and 12 % for VIIRS and MODIS respectively) and suggests that no specific algorithm is required north of the Sea Ice Extend front ($\sim$ 60 °S). With our dataset, OCI performs better than SO-specific algorithm in the SIZ (offset of $\sim$20 % for OCI and $\sim$45 % for SPGANTv4). This might be explained by the sub-region and seasons used to develop these algorithms (not representative of the whole SIZ), however more matchups are needed to better constrain the relationship. While float data have significant uncertainties in estimating chla and POC, the large dynamic range in the SO and consistency in the data support the use of profiling floats for validation of satellite-based biogeochemical algorithm performance. POC derived from MODIS and VIIRS agrees well with the float product within the uncertainty specified. The biogeochemical data set from our pre-SOCCOM and SOCCOM autonomous floats is consistent with OC products (chla, POC) and can be used as the third dimension (depth) and provide winter coverage to complement remote sensing in the Southern Ocean.

REFERENCES

Bailey, S. W., and P. J. Werdell (2006), A multi-sensor approach for the on-orbit validation of ocean color satellite data products, *Remote Sensing of Environment*, *102*(1-2), 12–23, doi:10.1016/j.rse.2006.01.015.

Behrenfeld, M. J., E. Boss, D. A. Siegel, and D. M. Shea (2005), Carbon-based ocean productivity and phytoplankton physiology from space, *Global Biogeochemical Cycles*, *19*(1), 1–14, doi:10.1029/2004GB002299.

Behrenfeld, M. J., Y. Hu, R. T. O'Malley, E. S. Boss, C. A. Hostetler, D. A. Siegel, J. L. Sarmiento, J. Schulien, J. W. Hair, X. Lu, S. Rodier, and A. J. Scarino (2016), Annual boom-bust cycles of polar phytoplankton biomass revealed by space-based lidar, *Nature Geoscience*, *10*(2), 118–122, doi:10.1038/ngeo2861.

Boss, E., and W. S. Pegau (2001), Relationship of light scattering at an angle in the backward direction to the backscattering coefficient, *Applied Optics*, *40*(30), 5503, doi:10.1364/AO.40.005503.

Boss, E., M. Picheral, T. Leeuw, A. Chase, E. Karsenti, G. Gorsky, L. Taylor, W. Slade, J. Ras, and H. Claustre (2013), The characteristics of particulate absorption, scattering and attenuation coefficients in the surface ocean; Contribution of the Tara Oceans expedition, *Methods in Oceanography*, *7*, 52–62, doi:10.1016/j.mio.2013.11.002.

Brainerd, K. E., and M. C. Gregg (1995), Surface mixed and mixing layer depths, *Deep-Sea Research Part I*, *42*(9), 1521–1543, doi:10.1016/0967-0637(95)00068-H.

Cetinić, I., M. J. Perry, N. T. Briggs, E. Kallin, E. A. D'Asaro, and C. M. Lee (2012), Particulate organic carbon and inherent optical properties during 2008 North Atlantic bloom experiment, *Journal of Geophysical Research: Oceans*, *117*(6), doi:10.1029/2011JC007771.

Cullen, J. J. (1982), The deep chlorophyll maximum: comparing vertical profiles of chlorophyll, *Deep Sea Research Part B. Oceanographic Literature Review*, *29*(12), 787, doi:10.1016/0198-0254(82)90274-6.

Cullen, J. J. (2015), Subsurface Chlorophyll Maximum Layers: Enduring Enigma or Mystery Solved?, *Annual Review of Marine Science*, *7*(1), 207–239, doi:10.1146/annurev-marine-010213-135111.

Dierssen, H. M. (2010), Perspectives on empirical approaches for ocean color remote sensing of chlorophyll in a changing climate, *Proceedings of the National Academy of Sciences*, *107*(40), 17,073–17,078, doi:10.1073/pnas.0913800107.

Dierssen, H. M., and R. C. Smith (2000), Bio-optical properties and remote sensing ocean color algorithms for Antarctic Peninsula waters, *Journal of Geophysical Research: Oceans*, *105*(C11), 26,301–26,312, doi:10.1029/1999JC000296.

Frölicher, T. L., J. L. Sarmiento, D. J. Paynter, J. P. Dunne, J. P. Krasting, and M. Winton (2015), Dominance of the Southern Ocean in Anthropogenic Carbon and Heat Uptake in CMIP5 Models, *Journal of Climate*, *28*(2), 862–886, doi:10.1175/JCLI-D-14-00117.1.

Gordon, H. R., and D. K. Clark (1980), Remote sensing optical properties of a stratified ocean: an improved interpretation, *Applied Optics*, *19*(20), 3428, doi:10.1364/AO.19.003428.

Graff, J. R., T. K. Westberry, A. J. Milligan, M. B. Brown, G. Dall'Olmo, V. van Dongen-Vogels, K. M. Reifel, and M. J. Behrenfeld (2015), Analytical phytoplankton carbon measurements spanning diverse ecosystems, *Deep Sea Research Part I: Oceanographic Research Papers*, *102*, 16–25, doi:10.1016/j.dsr.2015.04.006.

Guinet, C., X. Xing, E. Walker, P. Monestiez, S. Marchand, B. Picard, T. Jaud, M. Authier, C. Cotté, A. C. Dragon, E. Diamond, D. Antoine, P. Lovell, S. Blain, F. D'Ortenzio, and H. Claustre (2013), Calibration procedures and first dataset of Southern Ocean chlorophyll a profiles collected by elephant seals equipped with a newly developed CTD-fluorescence tags, *Earth System Science Data*, *5*(1), 15–29, doi:10.5194/essd-5-15-2013.

Holm-Hansen, O., M. Kahru, C. Hewes, S. Kawaguchi, T. Kameda, V. Sushin, I. Krasovski, J. Priddle, R. Korb, R. Hewitt, and B. Mitchell (2004), Temporal and spatial distribution of chlorophyll-a in surface waters of the Scotia Sea as determined by both shipboard measurements and satellite data, *Deep Sea Research Part II: Topical Studies in Oceanography*, *51*(12-13), 1323–1331, doi:10.1016/j.dsr2.2004.06.004.

Hooker, S. B., L. Van Heukelem, C. S. Thomas, H. Claustre, J. Ras, R. Barlow, H. Sessions, L. Schlueter, J. Perl, C. Trees, V. Stuart, E. Head, L. Clementson, J. Fishwick, C. Llewellyn, and J. Aiken (2005), The Second SeaWiFS HPLC analysis Round-Robin experiment (SeaHARRE-2), *NASA Tech. Memo,Goddard Space Flight Center*, *2005-21278*(August), 112pp.

Hooker, S. B., L. Van Heukelem, C. Thomas, H. Claustre, J. Ras, L. Schluter, L. Clementson, D. Van Der Linde, E. Eker-Develi, J.-F. Berthon, R. Barlow, H. Sessions, H. Ismail, and J. Perl (2009), The Third SeaWiFS HPLC Analysis Round-Robin Experiment (SeaHARRE-3), *NASA Tech. Memo,Goddard Space Flight Center*, *2009-21584*.

Hu, C., Z. Lee, and B. Franz (2012), Chlorophyll a algorithms for oligotrophic oceans: A novel approach based on three-band reflectance difference, *Journal of Geophysical Research: Oceans*, *117*(C1), n/a–n/a, doi:10.1029/2011JC007395.

IOCCG (2011), Bio-Optical Sensors on Argo Floats. Claustre, H. (ed.), *Reports of the International Ocean-Colour Coordinating Group, No. 11, IOCCG, Dartmouth, Canada.*

IOCCG (2015), Ocean Colour Remote Sensing in Polar Seas. Babin, M., Arrigo, K., Bélanger, S. and Forget, M-H. (eds.), *IOCCG Report Series, No. 16, International Ocean Colour Coordinating Group, Dartmouth, Canada.*

Johnson, K., and H. Claustre (2016), The scientific rationale, design, and implementation plan for a Biogeochemical-Argo float array, *Biogeochemical-Argo Planning Group*, doi:10.13155/46601.

Johnson, R., P. G. Strutton, S. W. Wright, A. McMinn, and K. M. Meiners (2013), Three improved satellite chlorophyll algorithms for the Southern Ocean, *Journal of Geophysical Research: Oceans*, *118*(7), 3694–3703, doi:10.1002/jgrc.20270.

Kahru, M., and B. G. Mitchell (2010), Blending of ocean colour algorithms applied to the Southern Ocean, *Remote Sensing Letters*, *1*(2), 119–124, doi:10.1080/01431160903547940.

Kolber, Z., and P. G. Falkowski (1993), Use of active fluorescence to estimate phytoplankton photosynthesis in situ, *Limnology and Oceanography*, *38*(8), 1646–1665, doi:10.4319/lo.1993.38.8.1646.

Marrari, M., C. Hu, and K. Daly (2006), Validation of SeaWiFS chlorophyll a concentrations in the Southern Ocean: A revisit, *Remote Sensing of Environment*, *105*(4), 367–375, doi:10.1016/j.rse.2006.07.008.

Martinez-Vicente, V., G. Dall'Olmo, G. Tarran, E. Boss, and S. Sathyendranath (2013), Optical backscattering is correlated with phytoplankton carbon across the Atlantic Ocean, *Geophysical Research Letters*, *40*(6), 1154–1158, doi:10.1002/grl.50252.

Mitchell, B. G., and O. Holm-Hansen (1991), Bio-optical properties of Antarctic Peninsula waters: differentiation from temperate ocean models, *Deep Sea Research Part A. Oceanographic Research Papers*, *38*(8-9), 1009–1028, doi:10.1016/0198-0149(91)90094-V.

Mitchell, B. G., and M. Kahru (2009), Bio-Optical Algorithms for ADEOS-2 GLI, *Journal of the Remote Sensing Society of Japan*, *29*(1), 80–85, doi:http://doi.org/10.11440/rssj.29.80.

Mobley, C. D., J. Werdell, B. Franz, Z. Ahmad, and S. Bailey (2016), Atmospheric Correction for Satellite Ocean Color Radiometry, A Tutorial and Documentation NASA Ocean Biology Processing Group.

Mueller, J. L., R. R. Bidigare, C. Trees, W. M. Balch, J. Dore, D. T. Drapeau, D. M. Karl, L. Van Heukelem, and J. Perl (2003), Ocean optics protocols for satellite ocean color sensor validation, Revision 5, Volume V: Biogeochemical and bio-optical measurements and data analysis protocols, *NASA Technical Memorandum*, *V*(2003- 211621, Rev. 5, vol. V), 36.

Muller, P., X. Li, and K. Niyogi (2001), Non-Photochemical quenching. A Reponse to excess Light energy., *Plant Physiology*, *125*(4), 1558–1566, doi:10.1104/pp.125.4.1558.

NASA Goddard Space Flight Center, O. E. L. O. B. P. G. (2014), MODIS-Aqua Level-2 Ocean Color Data Version 2014, doi:10.5067/AQUA/MODIS_OC.2014.0.

NASA Goddard Space Flight Center, O. E. L. O. B. P. G. (2015), VIIRS-NPP Level 2 Ocean Color Data Version 2014, doi:10.5067/NPP/VIIRS/L2/OC/2014.

Proctor, C. W., and C. S. Roesler (2010), New insights on obtaining phytoplankton concentration and composition from in situ multispectral Chlorophyll fluorescence, *Limnology and Oceanography: Methods*, *8*(Dickey 1991), 695–708, doi:10.4319/lom.2010.8.695.

Reda, I., and A. Andreas (2004), Solar position algorithm for solar radiation applications, *Solar Energy*, *76*(5), 577–589, doi:10.1016/j.solener.2003.12.003.

Ricker, W. E. (1973), Linear Regressions in Fishery Research, *Journal of the Fisheries Research Board of Canada*, *30*(3), 409–434, doi:10.1139/f73-072.

Sackmann, B. S., M. J. Perry, and C. C. Eriksen (2008), Seaglider observations of variability in daytime fluorescence quenching of chlorophyll-a in Northeastern Pacific coastal waters, *Biogeosciences Discussions*, *5*(4), 2839–2865, doi:10.5194/bgd-5-2839-2008.

Sarmiento, J. L., R. Slater, R. Barber, L. Bopp, S. C. Doney, A. C. Hirst, J. Kleypas, R. Matear, U. Mikolajewicz, P. Monfray, V. Soldatov, S. A. Spall, and R. Stouffer (2004), Response of ocean ecosystems to climate warming, *Global Biogeochemical Cycles*, *18*(3), n/a–n/a, doi:10.1029/2003GB002134.

Sathyendranath, S., V. Stuart, A. Nair, K. Oka, T. Nakane, H. Bouman, M. Forget, H. Maass, and T. Platt (2009), Carbon-to-chlorophyll ratio and growth rate of phytoplankton in the sea, *Marine Ecology Progress Series*, *383*, 73–84, doi:10.3354/meps07998.

Stramski, D., R. A. Reynolds, M. Babin, S. Kaczmarek, M. R. Lewis, R. Röttgers, A. Sciandra, M. Stramska, M. S. Twardowski, B. A. Franz, and H. Claustre (2008), Relationships between the surface concentration of particulate organic carbon and optical properties in the eastern South Pacific and eastern Atlantic Oceans, *Biogeosciences*, *5*(1), 171–201, doi:10.5194/bg-5-171-2008.

Sullivan, C. W., K. R. Arrigo, C. R. McClain, J. C. Comiso, and J. Firestone (1993), Distributions of phytoplankton blooms in the Southern Ocean, *Science*, *262*(5141), 1832–1837, doi:10.1126/science.262.5141.1832.

Sullivan, J. M., M. S. Twardowski, J. Ronald, V. Zaneveld, and C. C. Moore (2013), Measuring optical backscattering in water, in *Light Scattering Reviews 7*, edited by A. A. Kokhanovsky, no. ISBN 978-3-642-10335-3 in Springer Praxis Books, pp. 189–224, Springer Berlin Heidelberg, Berlin, Heidelberg, doi:10.1007/978-3-642-21907-8_6.

Thomalla, S. J., A. G. Ogunkoya, M. Vichi, and S. Swart (2017), Using optical sensors on gliders to estimate phytoplankton carbon concentrations and Chlorophyll-to-carbon ratios in the Southern Ocean, *Frontiers in Marine Science*, *4*(February), 1–19, doi:10.3389/fmars.2017.00034.

Van Heukelem, L., and C. S. Thomas (2001), Computer-assisted high-performance liquid chromatography method development with applications to the isolation and analysis of phytoplankton pigments, *Journal of Chromatography A*, *910*(1), 31–49, doi:10.1016/S0378-4347(00)00603-4.

Werdell, P. J., and S. W. Bailey (2005), An improved in-situ bio-optical data set for ocean color algorithm development and satellite data product validation, *Remote Sensing of Environment*, *98*(1), 122–140, doi:10.1016/j.rse.2005.07.001.

Xing, X., A. Morel, H. Claustre, D. Antoine, F. D'Ortenzio, A. Poteau, and A. Mignot (2011), Combined processing and mutual interpretation of radiometry and fluorimetry from autonomous profiling Bio-Argo floats: Chlorophyll a retrieval, *Journal of Geophysical Research*, *116*(C6), C06,020, doi:10.1029/2010JC006899.

Xing, X., H. Claustre, S. Blain, F. D'Ortenzio, D. Antoine, J. Ras, and C. Guinet (2012), Quenching correction for in vivo chlorophyll fluorescence acquired by autonomous platforms: A case study with instrumented elephant seals in the Kerguelen region (Southern Ocean), *Limnology and Oceanography: Methods*, *10*(7), 483–495, doi:10.4319/lom.2012.10.483.

Xing, X., H. Claustre, E. Boss, C. Roesler, E. Organelli, A. Poteau, M. Barbieux, and F. D'Ortenzio (2017), Correction of profiles of in-situ chlorophyll fluorometry for the contribution of fluorescence originating from non-algal matter, *Limnology and Oceanography: Methods*, *15*(1), 80–93, doi:10.1002/lom3.10144.

Zaneveld, J. R. V., A. H. Barnard, and E. Boss (2005), Theoretical derivation of the depth average of remotely sensed optical parameters, *Optics Express*, *13*(22), 9052, doi:10.1364/OPEX.13.009052.

Zhang, X., L. Hu, and M.-X. He (2009), Scattering by pure seawater: Effect of salinity, *Optics Express*, *17*(7), 5698–5710, doi:10.1364/OE.17.012685.

BIOGRAPHY OF THE AUTHOR

Nils Haëntjens is born in Paris, France the 9th of July 1991. He went to high school at Sainte Geneviève in Asnières-sur-Seine, France before completing a Master's Degree of Engineer in Embedded Systems at l'Institut Supérieur d'Electronique de Paris (ISEP) in 2014. Nils Haëntjens is a candidate for the Master of Science degree in Oceanography from The University of Maine in May 2017.